

# Coupling of Dual Mass-Transferring White-Dwarf Binaries as a Variable Gravitational-Wave Emitter

Naoki Seto

*Department of Physics, Kyoto University, Kyoto 606-8502, Japan*

8 July 2020

## ABSTRACT

We study evolution of a hierarchical four-body (2+2) system composed by a pair of mass-transferring white dwarf binaries. Applying a simplified model around the synchronous state of two inner orbital periods, we newly find that the four body system could settle down to a limit cycle with a small period gap. The period gap generates an amplitude variation of emitted gravitational waves, as a beat effect. Depending on model parameters, the beat period could be 1-10 yr and a large amplitude variation might be observed by space gravitational-wave detectors.

**Key words:** gravitational waves – celestial mechanics – stars: binaries: close – stars: kinematics and dynamics

## 1 INTRODUCTION

Synchronization phenomena have been widely observed in various research fields, including physics, chemistry and biology (Pikovsky et al. 2003). So far, sound waves had been a quite efficient messenger for identifying synchronized states. For example, in 1665, Huygens discovered a synchronization capture of two coupled pendulum-clocks emitting ticking sounds. The emergence of synchronized clapping is another well-known example related to sound waves (Néda et al. 2000).

After the detection of GW150914 by advanced-LIGO, gravitational wave measurements have rapidly become a powerful tool for physics and astronomy (Abbott et al. 2016). In general, binaries are considered to be promising sources of gravitational radiation in broad frequency regime. In the context of gravitational wave astronomy, Seto (2018) studied possibility of synchronization capture for hierarchical four-body (2+2) system composed by two inner binaries (see also Breiter & Vokrouhlický 2018; Tremaine 2020 for resonant interactions between inner binaries). He pointed out that mass-transferring white dwarf (WD) binaries (AM-CVn stars) could be intriguing systems for realizing a synchronized state in the LISA band. This is because of the self-regulated nature of their mass transfers. More specifically, in contrast to a binary effectively formed by two point masses (e.g. binary black holes), the time-dependent mass transfer rate can efficiently soften the response of inner angular velocity to externally added torque. Seto (2018) also found that, after the synchronization capture, the luminosity of gravitational radiation will decrease significantly, due to the phase cancellation of the two coupled wave sources.

Furthermore, a parasitic relation between the two binaries will be a likely outcome, and one of the two binaries seizes angular momentum from the other, with the assistance of the synchronization.

LISA is expected to detect  $10^3$ - $10^4$  isolated mass-transferring WD binaries (Nelemans, Yungelson & Portegies Zwart 2004). One might be further interested in the formation scenarios of a hierarchical 2+2 system composed by two WD binaries. In the main sequence stage, for nearby solar-type (F and G) dwarfs, the fraction of hierarchical 2+2 systems is estimated to be  $\sim 4\%$  of the total systems (Tokovinin 2014; see also Raghavan et al. 2010). The observed multiplicity fraction is known to be generally higher for more massive stars such as the O-type stars (Sana et al. 2013). However, during the stellar evolution, we need significant shrinkages of the inner and outer orbits to make the compact 2+2 systems as studied in Seto (2018) and also in this paper.

In the case of an isolated WD binary, the common-envelope (CE) phase is considered to be important for its orbital contraction. But, its basic physical processes are not well understood at present (for reviews see e.g. Iben & Livio 1993; Taam & Sandquist 2000). Compared with binaries, the effects of the CE phases would be much more complicated for triple and quadrupole systems (for triple systems, see e.g. de Vires et al. 2014, Toonen et al. 2016; Glanz & Perets 2020). From a pessimistic perspective, there is a possibility that, in many cases, the 2+2 structure might not be maintained during the CE phases (as naively speculated from Glanz & Perets 2020). But, considering the large uncertainties, it would be currently difficult to make solid discussions on the roles of the CE phases for 2+2 systems.

In this paper, as in Seto (2018), we rather concentrate

arXiv:2007.03176v1 [astro-ph.HE] 7 Jul 2020

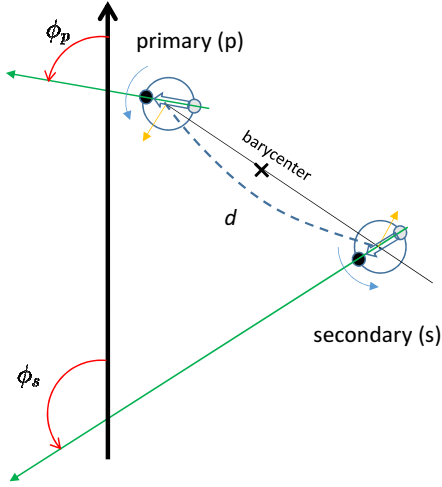


**Figure 1.** The geometry of dual mass-transferring WD-WD binaries (p: primary and s: secondary) aligned on the same plane. The gray circles show the lighter components in the two binaries ( $m_{p2}$  and  $m_{s2}$ ) corresponding to the donors of mass transfers. The orientation angles  $\phi_p$  and  $\phi_s$  are measured relative to the fixed direction (thick solid line). We define the relative angle  $\Delta \equiv \phi_s - \phi_p$ . The outer orbital distance is  $d$  and the inner semi-major axes are given by  $a_p$  and  $a_s$ . The three orbits are assumed to be circular.

on the evolution of coupled two mass-transferring WD binaries only around the synchronization states. To extract essential degrees of freedom and keep robustness of our discussion, we use a very simple model for conservative mass transfers, based on Paczyński (1967) and Paczyński & Sienkiewicz (1972). We exclude all the details added in later studies (e.g. spin effects).

In this paper, as contrasted to the synchronization capture studied in Seto (2018), we newly report the existence of a limit cycle for gravitationally coupled two WD binaries. In this state, the two binaries keep slightly different angular velocities and periodically change gravitational wave luminosity as a beat effect. Depending on model parameters, the beat period could become 1-10 yr and might be actually observed by space gravitational-wave interferometers such as LISA, TianQin and Taiji.

## 2 BASIC EQUATIONS

We study evolution of a hierarchical four-body system composed by two mass-transferring WD binaries, as illustrated in Fig. 1. We assume that the three (one outer and two inner) orbits are circular and aligned on the same plane (see also Fang, Thompson, & Hirata 2017; Hamers & Lai 2017; Fragione & Kocsis 2019 for possible effects of inclination). We put the total masses of the two binaries by  $M_p$  (p: primary) and  $M_s$  (s: secondary) with  $M_p > M_s$ , and denote their mutual distance by  $d$  (see Fig. 1). We use the angles ( $\phi_p, \phi_s$ ) to represent the orientations of the binaries relative to a fixed direction (Fig. 1). Then, we define the relative orientation angle  $\Delta \equiv \phi_s - \phi_p$  which plays an important role in this paper.

This section is organized in the following order. In §2.1, we describe our model for the inner orbits. In §2.2, we mention coupling between the two binaries and present resonant terms. In §2.3, we summarize differential equations used for our numerical calculations. Then, in §2.4, we derive some expressions that will be useful to interpret our numerical results.

### 2.1 INNER BINARIES

In this subsection, we mainly discuss the primary binary, but we will apply our results equally to the secondary binary, after changing subscripts.

We put individual masses of the primary binary by  $m_{p1}$  and  $m_{p2}$  with  $m_{p1} > m_{p2}$  and  $M_p = m_{p1} + m_{p2}$ . The reduced mass is given by  $\mu_p \equiv m_{p1}m_{p2}/M_p$  and the mass ratio by  $q_p \equiv m_{p2}/m_{p1} < 1$ . With its semi-major axis  $a_p$ , the orbital angular velocity of the primary is given by

$$n_p \equiv \dot{\phi}_p = (GM_p/a_p^3)^{1/2}, \quad (1)$$

and its quadrupole moment is expressed as

$$\mu_p a_p^2 = G^{2/3} \mathcal{M}_p^{5/3} n_p^{-4/3} \quad (2)$$

with the chirp mass  $\mathcal{M}_p \equiv \mu_p^{3/5} M_p^{2/5}$ .

The orbital angular momentum of the primary binary is written by

$$J_p = \mu_p (GM_p a_p)^{1/2} = \mu_p a_p^2 n_p. \quad (3)$$

In the following, we deal with conservative mass transfer (i.e.  $\dot{M}_p = \dot{m}_{p1} + \dot{m}_{p2} = 0$ ). We will shortly explain a concrete model for the rate  $\dot{m}_{p2}$ . From Eq. (3), we have

$$\frac{\dot{J}_p}{J_p} = \frac{1}{2} \frac{\dot{a}_p}{a_p} + \frac{\dot{m}_{p2}}{m_{p2}} (1 - q_p). \quad (4)$$

The binary emits gravitational radiation mainly at the wavelength  $\lambda_p = \pi c/n_p$  (frequency:  $n_p/\pi$ ). If the coupling between the two binaries are negligible, the rate of angular momentum loss is given by (e.g. Maggiore 2008)

$$(\dot{J}_p)_{\text{gw}} = Y_{\text{pp}} = -\frac{32G a_p^4 n_p^5 \mu_p^2}{5c^5}. \quad (5)$$

The associated timescale is given by

$$\begin{aligned} t_{\text{gw},p} &\equiv -\left[\frac{(\dot{J}_p)_{\text{gw}}}{J_p}\right]^{-1} = \frac{5c^5}{32G^{5/3} \mathcal{M}_p^{5/3} n_p^{8/3}} \\ &= 1.5 \times 10^8 \left(\frac{\mathcal{M}_p}{0.133 M_\odot}\right)^{-5/3} \left(\frac{n_p}{0.005 \text{ s}^{-1}}\right)^{-8/3} \text{ yr}. \end{aligned} \quad (6)$$

Next, we move to discuss the mass transfer rate within each binary. We follow Paczyński (1967) and Paczyński & Sienkiewicz (1972) for the Roche lobe overflow within a white dwarf binary. For the equation of state of WDs, we use the polytropic model with the index 3/2 for non-relativistic degenerate gas, and the mass-radius relation is given by ( $i = 1, 2$ )

$$R_{pi} = 0.0126 R_\odot \left(\frac{m_{pi}}{1 M_\odot}\right)^{-1/3} \quad (7)$$

(see e.g., Zappolisky & Salpeter 1969 for a more detailed modeling). From Eq. (7), we have  $R_{p2} > R_{p1}$  and the lighter

component of the binary is the donor with  $\dot{m}_{p2} < 0$ . We estimate its Roche lobe radius by (Paczynski 1967)

$$R_{Lp2} = \frac{2a}{3^{4/3}} \left( \frac{m_{p2}}{M_p} \right)^{1/3}. \quad (8)$$

The mass transfer is stable for the condition  $d(R_{Lp2}/R_{p2})/dm_{p2} < 0$  (for  $J_p = \text{const}$ ) and this can be simplified as  $q_p = m_{p2}/m_{p1} < 2/3$  (see e.g. Paczynski 1967; Solheim 2010). We use the mass transfer rate

$$\frac{\dot{m}_{p2}}{m_{p2}} = -2n \left( \frac{R_{p2} - R_{Lp2}}{R_{p2}} \right)^3 \theta(R_{p2} - R_{Lp2}) \quad (9)$$

given by the competition between  $R_{Lp2}$  and  $R_{p2}$  with the step function  $\theta(\cdot)$  (Paczynski & Sienkiewicz 1972; Webbink 1984, see also Marsh, Nelemans & Steeghs 2004). In fact, the step function plays no role for most of our numerical calculations below (except for §3.2). It should be also noticed that, in our study, as long as our modeling is valid, the compact accreter is not necessarily a white dwarf. But, at least for isolated binaries, LISA is likely to detect double white dwarf binaries much more than binaries including neutron stars or black holes (see e.g. Nelemans et al. 2001).

The stable and self-regulated mass transfer (9) is crucially important for our study. It softens the response of angular velocity  $n_p$ , against externally added torque, resulting in dynamically interesting phenomena. During the mass transfer phase, the binary satisfies the relation

$$0 < R_{p2} - R_{Lp2} \ll R_{p2}. \quad (10)$$

Then, from Eqs. (1)(7) and (8) the donor mass  $m_{p2}$  is approximately given by the angular velocity  $n_p$  as

$$m_{p2} \simeq 0.036 \left( \frac{n_p}{0.005 \text{ s}^{-1}} \right) M_\odot. \quad (11)$$

For an isolated binary, at quasi-steady state of mass transfer  $\dot{m}_{p2} \simeq 0$ , we have (Gokhale, Peng & Frank 2007)

$$\frac{\dot{a}_p}{a_p} = -\frac{2}{3} \frac{\dot{n}_p}{n_p} = -\frac{2}{3} \frac{\dot{m}_{p2}}{m_{p2}} = \left( 1 - \frac{3}{2} q_p \right)^{-1} t_{\text{gw},p}^{-1}. \quad (12)$$

In §3, we use this relation to set up the initial conditions for our numerical calculations.

## 2.2 COUPLING BETWEEN TWO BINARIES

We now discuss gravitational coupling between two binaries around the synchronization state  $\Delta = n_s - n_p \simeq 0$ . We extract the relevant resonant terms caused by the Newtonian tidal interaction and the gravitational radiation reaction. The former is the leading order term of the conservative effects and the latter is that of the dissipative effects. Throughout this paper, we assume that the four-body system is in the near zone ( $d \ll \lambda_p \simeq \lambda_s$ ), and ignore the time retardation for the couplings. We also put aside short-duration terms that depend on rapidly changing angular variables. But these terms might play certain roles in some cases.

Due to the Newtonian tidal interaction with the secondary, the primary receives the following resonant torque

$$T_p = \frac{9Ga_p^2 a_s^2 \mu_p \mu_s}{16d^5} \sin(2\Delta). \quad (13)$$

This expression is consistent with Tremaine (2020). The secondary receives the counter torque  $T_s = -T_p$ . Given the

conjugate structure of the variables, these terms are not directly related to the time variation of eccentricities (Murray & Dermott 1999).

Next, we deal with the coupling between the two binaries due to the gravitational radiation reaction. In most situations, such effect is totally negligible. But, for our systems with  $d \ll \lambda_p \simeq \lambda_s$ , the coherent nature could be exceptionally workable. From the Burke-Thorne potential (Thorne 1969; Burke 1971; Maggiore 2008), the radiational torque on the primary due to the secondary is estimated to be

$$Y_{ps} = -\frac{32Ga_p^2 a_s^2 n_s^5 \mu_p \mu_s}{5c^5} \cos(2\Delta). \quad (14)$$

Similarly, the secondary receives the following torque

$$Y_{sp} = -\frac{32Ga_s^2 a_p^2 n_p^5 \mu_p \mu_s}{5c^5} \cos(2\Delta). \quad (15)$$

## 2.3 EQUATIONS FOR NUMERICAL STUDIES

In this subsection, for a preparation of numerical calculations, we summarize expressions provided so far. Hereafter, for notational conciseness, we put  $n_p = n_s = n$  ( $\lambda_p = \lambda_s = \lambda$ ), unless the difference between  $n_p$  and  $n_s$  should be clarified.

First, we write down the total torque for each binary. From Eqs. (5)(13)(14) and (15), we have

$$\frac{\dot{J}_p}{J_p} = \frac{Y_{pp} + Y_{ps} + T_p}{J_p} \quad (16)$$

$$= -\frac{1}{t_{\text{gw},s}} [F + \cos(2\Delta) - D \sin(2\Delta)] \quad (17)$$

$$\frac{\dot{J}_s}{J_s} = \frac{Y_{ss} + Y_{sp} + T_s}{J_s} \quad (18)$$

$$= -\frac{1}{t_{\text{gw},s}} [1 + F \cos(2\Delta) + DF \sin(2\Delta)] \quad (19)$$

for the primary and secondary. Here we introduced the following two parameters that will become important in the rest of this paper

$$F \equiv \left( \frac{M_p}{M_s} \right)^{5/3}, \quad (20)$$

$$D \equiv \frac{45c^5 n^{-5}}{2^9 d^5} = \frac{45}{512\pi^5} \left( \frac{\lambda}{d} \right)^5 \quad (21)$$

$$= 36.2 \left( \frac{n}{0.005 \text{ s}^{-1}} \right)^{-5} \left( \frac{d}{0.12 \text{ AU}} \right)^{-5}.$$

In the absence of the coupling terms, we have  $F = \dot{n}_p/\dot{n}_s \geq 1$  for the two angular speeds. To reduce the encounter speed  $\propto (F-1)$  and thereby enhance dynamical interaction around the synchronization condition  $\dot{\Delta} \sim 0$ , we numerically study the cases with  $0 < F - 1 \ll 1$ . Meanwhile, the parameter  $D$  represents the strength of the Newtonian torque relative to the radiative ones. Its prefactor  $45/(512\pi^6) \sim 3 \times 10^{-4}$  is much smaller than unity. Considering the requirement  $\lambda \gg d$ , we mainly study the range  $D \gtrsim 10$ .

We also need to take into account the orbital stability for the four-body system. We apply the stability criterion in Mardling & Aarseth (2001) by considering an effective triple system composed the secondary binary (masses  $m_{s1}$  and  $m_{s2}$ ) and the third body of the primary's total mass

$M_p$ . Then, for  $M_p \sim m_{s1} + m_{s2}$ , we obtain the upper limit for the coupling parameter

$$D_{\max} \sim 6.0 \times 10^8 \left( \frac{n}{0.005 \text{ s}^{-1}} \right)^{-5/3}. \quad (22)$$

In what follows, we examine the regime  $D \ll D_{\max}$ .

In our numerical calculations, we trace the time evolution of the five variables  $\Delta$ ,  $a_p$ ,  $a_s$ ,  $m_{p2}$  and  $m_{s2}$ , using the five differential equations below. From the balance of angular momenta, we have

$$\frac{1}{2} \frac{\dot{a}_p}{a_p} + \frac{\dot{m}_{p2}}{m_{p2}} (1 - q_p) = -\frac{1}{t_{\text{gw},s}} [F + \cos(2\Delta) - D \sin(2\Delta)], \quad (23)$$

$$\frac{1}{2} \frac{\dot{a}_s}{a_s} + \frac{\dot{m}_{s2}}{m_{s2}} (1 - q_s) = -\frac{1}{t_{\text{gw},s}} [1 + F \cos(2\Delta) + DF \sin(2\Delta)]. \quad (24)$$

From the definition of the relative angle  $\Delta$ , we have

$$\dot{\Delta} = \dot{\phi}_s - \dot{\phi}_p = \left( \frac{GM_s}{a_s^3} \right)^{1/2} - \left( \frac{GM_p}{a_p^3} \right)^{1/2}. \quad (25)$$

In addition, we use Eq. (9) for the mass transfer rate  $\dot{m}_{p2}$  and a similar one for  $\dot{m}_{s2}$ .

## 2.4 ENERGY EQUATION

As in Seto (2018), an energy equation for  $\Delta$  is useful to understand evolution of the coupled four-body system (see also Goldreich & Peale 1968; Murray & Dermott 1999 for another example). Here, we briefly discuss the basic aspects of the energy equation. From Eq. (1), we have

$$\ddot{\Delta} = \dot{n}_s - \dot{n}_p = -\frac{3n}{2} \left( \frac{\dot{a}_s}{a_s} - \frac{\dot{a}_p}{a_p} \right). \quad (26)$$

In the right-hand side of this expression, we dropped a correction of  $O[(n_p - n_s)/n]$ . Then, using Eqs. (23) and (24), we obtain

$$\begin{aligned} \ddot{\Delta} &= \frac{3n}{t_{\text{gw},s}} [(1 - F)(1 - \cos 2\Delta) + D(F + 1) \sin 2\Delta] \\ &= 3n \left[ \frac{\dot{m}_{s2}}{m_{s2}} (1 - q_s) - \frac{\dot{m}_{p2}}{m_{p2}} (1 - q_p) \right]. \end{aligned} \quad (27)$$

Multiplying  $\dot{\Delta}$  and integrating with time, we obtain

$$\frac{1}{2} \dot{\Delta}^2 + V(\Delta) = E(t), \quad (28)$$

where the potential  $V(\Delta)$  is given by

$$V(\Delta) \equiv \frac{3n}{2t_{\text{gw},s}} [(F - 1)(2\Delta - \sin 2\Delta) + D(F + 1) \cos 2\Delta]. \quad (29)$$

Here, we ignored the time variations of the parameters  $(n, F, D, t_{\text{gw},s})$ , since we are interested in a time period much shorter than  $t_{\text{gw},s}$ . Similarly, the total energy  $E(t)$  can be evaluated by

$$E(t) = E(0) + 3n \int_0^t dt \left[ \frac{\dot{m}_{s2}}{m_{s2}} (1 - q_s) - \frac{\dot{m}_{p2}}{m_{p2}} (1 - q_p) \right] \dot{\Delta} \quad (30)$$

with an integral constant  $E(0)$ . This expression shows that the total energy  $E(t)$  is changed by the mass transfers. For numerical evaluation of  $E(t)$ , we exclusively apply the left-hand side of Eq. (28), and use Eq. (30) only for analytical studies.

As mentioned earlier, we mainly analyze coupled binaries with  $0 < F - 1 \ll 1$  and  $D \gg 1$ . For such parameters, in Eq. (29), the local profile of the potential  $V(\Delta)$  is dominated by the term  $\propto D(F + 1) \cos 2\Delta$  with a small gradient  $\propto 2(F - 1)\Delta$ .

## 3 NUMERICAL RESULTS

We now numerically study the time evolution of two mass-transferring WD binaries, gravitationally coupled at the distance  $d$ . In this section, we assign various coupling parameters  $D$ , but unless otherwise stated, other conditions are identical (except for the last paragraph in §3.4). More specifically, we put  $(M_p, M_s) = (1.0M_\odot, 0.9M_\odot)$  and use the common initial conditions (at  $t = 0$ );  $\Delta = 0$ ,  $n_s = 5 \times 10^{-3} \text{ s}^{-1}$  and  $n_p = (1 + 2 \times 10^{-5})n_s$ . We finely adjust the initial donor masses  $(m_{p2}, m_{s2})$  to individually satisfy the third equality in Eq. (12) that is originally given for an isolated binary. Roughly speaking, for  $n_p \sim n_s \sim 5 \times 10^{-3} \text{ s}^{-1}$ , we have  $m_{p2} \sim m_{s2} \sim 0.036M_\odot$  (accordingly  $M_p \sim 0.133M_\odot$ ,  $M_s \sim 0.127M_\odot$ ,  $t_{\text{gw},s} \sim 1.6 \times 10^8 \text{ yr}$  and  $F \sim 1.046$ ).

### 3.1 OVERALL PHASE EVOLUTIONS

To begin with, we discuss the overall evolution of the phase difference  $\Delta$  for the four different coupling parameters  $D = 0.1, 24, 25$  and  $50$ . Here the parameter  $D = 0.1$  is not comfortably large, considering the near zone condition  $d \ll \lambda$ . We use this run just for a comparison.

In Fig. 2, we show our numerical results. In the early stage  $t \lesssim 20000 \text{ yr}$ , the coupling between the two binaries is non-resonant and inefficient. Therefore, in this stage, we will be able to make an extrapolation

$$\ddot{\Delta} \simeq \ddot{\Delta}_{\text{iso}}. \quad (31)$$

Here  $\ddot{\Delta}_{\text{iso}}$  is given by  $(\dot{n}_s - \dot{n}_p)$  for two isolated binaries as in Eq. (12), and its time variation can be neglected for the timescale under discussion. Integrating Eq. (31) twice and using the initial condition  $\Delta(0) = 0$ , we obtain a parabolic equation as an approximation to  $\Delta(t)$

$$\Delta_{\text{pb}}(t) = \frac{1}{2} \ddot{\Delta}_{\text{iso}} \times (t - 2t_c)t. \quad (32)$$

Here we defined the expected catch-up time for the two angular speeds

$$t_c = \frac{(n_p - n_s)_0}{\ddot{\Delta}_{\text{iso}}} \sim 2.6 \times 10^4 \text{ yr} \quad (33)$$

using the initial velocity difference  $(n_p - n_s)_0$ . We also denote the corresponding phase by

$$\Delta_c \equiv \Delta_{\text{pb}}(t_c) \sim -\frac{1}{2} \ddot{\Delta}_{\text{iso}} t_c^2 \sim -40000. \quad (34)$$

In fact, we set the initial difference  $(n_p - n_s)_0/n_{s0} = 2 \times 10^{-5}$  to have a large rotation cycles  $|\Delta_c|/(2\pi) \sim 10^4$ . Thus, around the critical epoch  $t \sim t_c$ , we will be able to suppress transient effects caused by our potentially artificial initial settings.

As shown in Fig. 2, depending weakly on  $D$ , the time profile  $\Delta(t)$  at  $0 < t \lesssim t_c$  is approximately given by the analytical expression (32). For  $D = 0.1$ , the coupling between the binaries are weak, even around  $t \sim t_c$ , and they merely

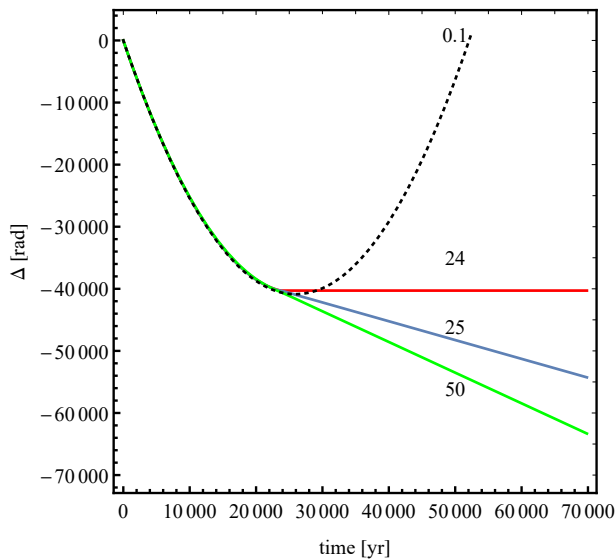


**Figure 2.** The time evolution of the phase angle  $\Delta$  for systems with various coupling parameters  $D$  (shown in the figure). At  $t \lesssim 20000$  yr, all of the four curves are nearly degenerated. For  $D = 0.1$ , the coupling between the two inner binaries is weak, and the system just passes through the synchronization point  $\dot{\Delta} = 0$ , globally approximated by the parabolic equation (32). The system with  $D = 24$  is captured into a synchronization state  $\Delta \sim 40286$ . For  $D = 25$  and  $50$ , the systems result in drifting solutions  $\dot{\Delta} \sim \text{const}$ .

pass through the resonant point  $\dot{\Delta} = 0$ , following the expression (32) still at  $t > t_c$ . In contrast, for  $D = 24, 25$  and  $50$ , we have quite different profiles  $\Delta(t)$  at  $t \gtrsim t_c$ . For  $D = 24$ , the binaries are captured into a synchronization state  $\Delta \sim 40286$  (as discussed in §3.2). Meanwhile, for  $D = 25$  and  $50$ , the systems asymptotically show constant drifts  $\dot{\Delta} \sim \text{const}$ .

Seto (2018) closely examined the success and failure of the synchronization capture (respectively corresponding to  $D = 24$  and  $0.1$  in Fig. 2). However, the existence of a drifting solution was not reported at all. Therefore, in this follow-on paper, we mainly discuss the drifting solutions (e.g.  $D = 25$  and  $50$ ), paying special attention to the boundary between the synchronization capture (e.g.  $D = 24$ ).

### 3.2 CAPTURE INTO SYNCHRONIZATION

First, as a comparison to the drifting solutions, we discuss the numerical run with  $D = 24$  resulted in synchronization capture. In Fig. 3, we plot its potential  $V(\Delta)$  and the total energy  $E(t)$  (red curve using Eq. (28)) around the synchronization capture. The red curve makes the first contact with the orange one (i.e.  $\dot{\Delta} = 0$ ) around  $\Delta = -40287.8$ , and  $\dot{\Delta}$  changes its sign from negative to positive.

Before this first contact, we have  $\dot{\Delta} < 0$  and the product  $[\dots] \times \dot{\Delta}$  in Eq. (30) has a negative mean, reducing the total energy  $E(t)$ . The wavy profile of the red curve in the bottom panel reflects the  $\Delta$ -dependence of the mass-transfer factor  $[\dots]$  in Eq. (30), mainly caused by the Newtonian angular momentum exchange. Following the arguments in Appendix A, we can see that this wavy component is approximately proportional to  $\sin 2\Delta$ .

In Fig. 3, after the first contact, the phase angle  $\Delta$  starts

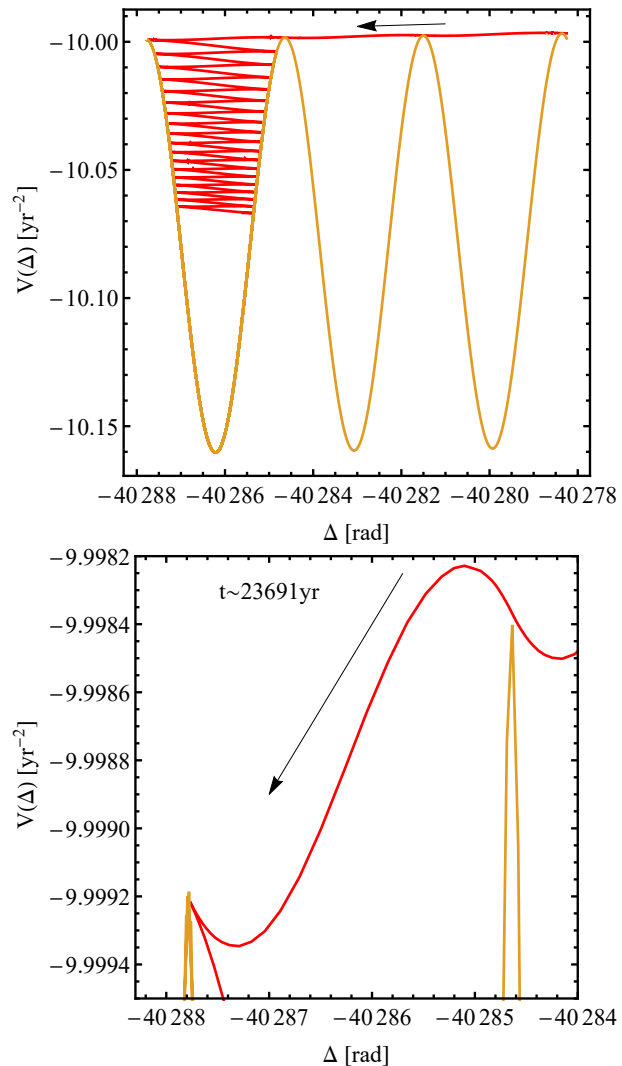


**Figure 3.** (Upper panel) The time evolution of the system with  $D = 24$  between  $t = 23678$ - $24024$  yr around the synchronization capture. The red curve shows the total energy  $E(t) = \dot{\Delta}^2/2 + V(\Delta)$ , relative to the potential  $V(\Delta)$  (orange curve). This system is captured into the synchronization state  $\Delta \simeq -40286.25$  (with  $\cos 2\Delta \simeq -1$ ). (Lower panel) An enlarged view of the upper panel around the first turning point at  $t \sim 23691$  yr.

to oscillates in the potential (see the upper panel). Now, the mass transfer factor  $[\dots]$  in Eq. (30) has an oscillating component in the anti-phase with  $\dot{\Delta}$ , efficiently decreasing the total energy  $E(t)$  down to the bottom of the potential ( $\cos 2\Delta \sim -1$ ). Along the way, the GW luminosity decreases significantly due to the phase cancellation, as reported in Seto (2018) (see also a related explanation in §4). Although we do not provide the corresponding numerical results here, the primary binary extracts the angular momentum of the secondary, realizing a parasitic relation with  $\dot{m}_{p2} = 0$  at  $t \gtrsim 3.8 \times 10^4$  yr (see Fig. 4 in Seto 2018 for a similar situation).

In the four runs shown in Fig. 2, except for the late stage of  $D = 24$ , we always have  $\dot{m}_{p2} < 0$  and  $\dot{m}_{s2} < 0$  simultaneously. Under these two inequalities, the step function in Eq. (9) plays no role, and can be omitted, when interpreting our numerical calculations.



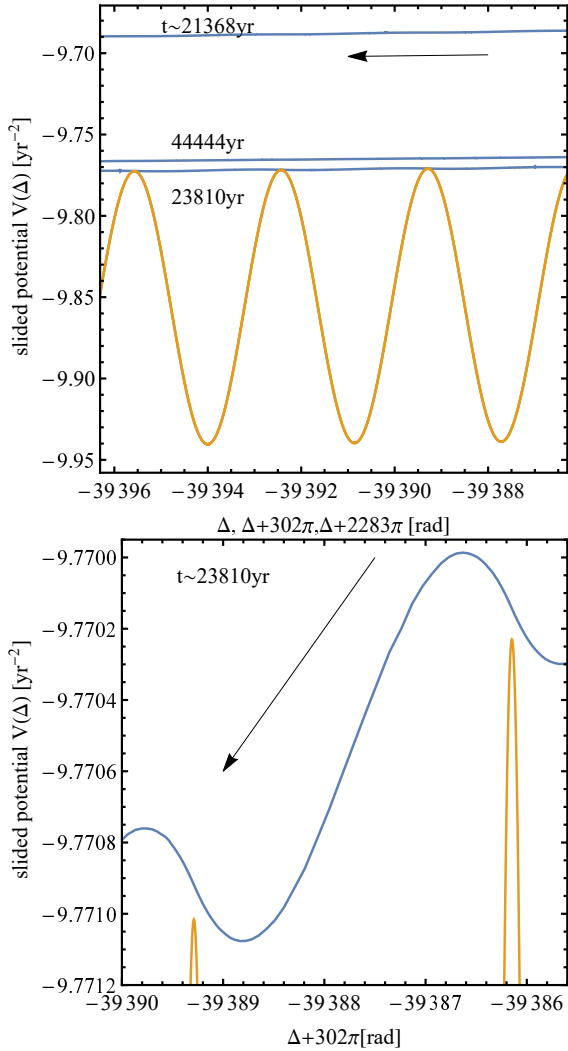


**Figure 4.** (Upper panel) The time evolution of the system with  $D = 25$  around three different epochs  $t \sim 21368, 23810$  and  $44444$  yr. The potential  $V(\Delta)$  (orange curve) is given for the total energy  $E(t)$  shown by the uppermost blue curve (labeled with 21368 yr). For the later two epochs, we appropriately slided both  $E(t)$  and  $V(\Delta)$ , to compare with the first epoch. (Lower panel) An enlarged view of Fig. 4 for the time evolution around 23810 yr. The blue curve does not contact with the orange curve, keeping  $\dot{\Delta} < 0$ .

### 3.3 DRIFTING SOLUTION

Next, we discuss the run with  $D = 25$ . As shown in Fig. 2, at the late stage  $t \gtrsim 30000$  yr, this system shows a nearly constant drift rate with the mean value

$$A \equiv |\bar{\dot{\Delta}}| = 0.303 \text{ yr}^{-1}. \quad (35)$$

In the upper panel of Fig. 4, we present the total energy  $E(t) = \dot{\Delta}^2/2 + V(\Delta)$  (the upper blue line) and the potential  $V(\Delta)$  (the orange curve) around  $t \sim 21368$  yr. At this relatively early stage, the system nearly keeps the initial acceleration  $\ddot{\Delta} = \ddot{\Delta}_{\text{iso}}$ , satisfying the parabolic equation (32) in the same way as other runs. In Fig. 4, the upper blue line has a slightly larger slope than that of the linear term  $3n(F-1)\Delta/t_{\text{gw},s}$  of the potential  $V(\Delta)$ , gradually decreasing the kinetic energy  $E(t) - V(\Delta)$ .

In the upper panel of Fig. 4, we added  $E(t)$  and  $V(\Delta)$  around  $t \sim 23810$  yr where two curves experienced the closest approach. Since the potential  $V(\Delta)$  effectively has a repetitive shape and only the relative position of the two curves are relevant for our study (showing  $\dot{\Delta}^2/2$ ), we commonly slided both  $E(t)$  and  $V(\Delta)$  in the horizontal and vertical directions, to directly compare with the situation at  $t \sim 21368$  yr mentioned earlier.

Because of the poor resolution of the upper panel of Fig. 4 in the vertical direction, the blue line appears to contact with the orange curve. But they are actually separated, as presented in the bottom panel. As in the case of the bottom panel of Fig. 3, we can see the wavy component  $\propto \sin 2\Delta$ .

Finally, in the upper panel of Fig. 4, during the drifting epoch around  $t \sim 44444$  yr, the energy  $E(t)$  shows a clear offset from the potential (again appropriately slided in the horizontal and vertical directions). This drifting solution can be regarded as a limit cycle sustained by the self-regulating mass transfer within two binaries (analytically examined in Appendix A).

In the upper panel of Fig. 4, comparing the chronological order of the three blue curves, the total energy  $E(t)$  does not change monotonically, relative to the potential  $V(\Delta)$ . But it bounces back to the upper direction, before relaxing to the limit cycle. This overshooting will become important in the next subsection.

For comparison, we also examine the transition point between the synchronization and the drifting solution, using different mass combinations  $(M_p, M_s) = (1.0M_\odot, 0.95M_\odot)$  and  $(1.0M_\odot, 0.85M_\odot)$ , still at  $n = 0.005 \text{ s}^{-1}$ . The parameter  $F \equiv (M_p/M_s)^{5/3}$  becomes 1.037 and 1.121 respectively, and we have transition at  $D = 5.9$  for the former and 59 for the latter. If we increase the total mass difference between two coupled WD-WD binaries, the intrinsic encounter speed  $\dot{\Delta}_{\text{iso}} \propto (F-1)$  increases, and we need a larger coupling parameter  $D$  to keep the system in a drifting solution. Similarly, for the coupling between a WD-WD binary and a WD-black hole binary, a much larger parameter  $D$  would be required for the drifting solution, because of a larger encounter speed  $\propto F-1$ .

### 3.4 DIFFERENCE BETWEEN $D = 24$ AND 25

As shown in Fig. 2, we have the distinct outcomes for  $D = 24$  and 25. The former is captured into synchronization, but the latter has a drifting solution. Here we briefly discuss the structure of their boundary, mainly from an interest in dynamical systems rather than from astronomical point of views.

One might imagine that, at  $D \lesssim 24$ , we no longer have a corresponding drifting solution. However, considering the overshooting of the blue curves in Fig. 4, it seems reasonable to presume that, even at  $D \sim 24$ , we still have a similar drifting solution, but the system in Fig. 3 was captured into synchronization state, by touching the potential curve and changing the sign of  $\dot{\Delta}$  (as a result of the overshooting observed in Fig. 4).

In order to clarify the existence of the drifting solution at  $D \lesssim 24$ , we performed a numerical experiment, artificially

changing the coupling parameter  $D$  as a function of time

$$D(t) = D_i + (D_f - D_i) \left[ \exp\left(\frac{t_t - t}{t_d}\right) + 1 \right]^{-1} \quad (36)$$

with  $D_i = 55$ ,  $D_f = 15$ ,  $t_t = 9.5 \times 10^4$  yr and  $t_d = 3.2 \times 10^4$  yr. This function smoothly connects two values from  $D \sim 55$  at  $t \ll t_t$  and  $D \sim 15$  at  $t \gg t_t$ . Our intention behind this numerical experiment can be explained as follows.

(i) We initially relax the system to a drifting solution with the large coupling parameter  $D = 55$ .

(ii) Then, using a relatively long transition time-scale  $t_d$  and suppressing the overshooting, we adiabatically lead the system down to  $D = 15$ .

With this function  $D(t)$ , we could indeed realize a drifting solution even for  $D = 15$ . Therefore, the difference between Figs. 3 and 4 and is not caused by disappearance of a valid limit cycle, but by the effect of the transient overshooting.

#### 4 VARIABLE GRAVITATIONAL WAVE AMPLITUDE

In this section, we discuss the time variation of gravitational wave amplitude, induced by the phase drift.

Considering the aligned orientation of the two coupled binaries, their quadrupole gravitational waves are written as

$$h_p(t) = hF \cos[2\phi_p(t)] = hF \cos[2\phi_s(t) - 2\Delta(t)], \quad (37)$$

$$h_s(t) = h \cos[2\phi_s(t)]. \quad (38)$$

Here the amplitudes  $h_p$  and  $h_s$  depend on various geometrical parameters, but their explicit form is not important for the present arguments. We also neglected the small Doppler effects induced by the outer orbital velocity. If the inter-binary separation  $d$  is smaller than the gravitational wavelength  $\lambda$  as assumed in this paper, the total signal is effectively given by

$$h_{\text{total}}(t) = h_p(t) + h_s(t). \quad (39)$$

For the drifting solution, the phase difference  $\Delta(t)$  in Eq. (37) changes much more slowly than the inner orbital angles  $\phi_s$ . Therefore, due to the beat effect, the total gravitational waveform changes its amplitude as follows

$$\mathcal{A}_{\text{total}} = h [1 + F^2 + 2F \cos 2\Delta(t)]^{1/2}. \quad (40)$$

The amplitude  $\mathcal{A}_{\text{total}}$  has a positive interference  $\mathcal{A}_{\text{total}} \sim h(F + 1)$  at  $\cos 2\Delta(t) = 1$ , but has a cancellation  $\mathcal{A}_{\text{total}} \sim h(F - 1)$  at  $\cos 2\Delta(t) = -1$ .

In this manner, the drifting solution would be interesting also from the viewpoint of gravitational wave observation. At the same time, we should notice that this amplitude variation is not merely an observational effect, but the intrinsic energy emission rate actually changes as  $\propto \mathcal{A}_{\text{total}}^2$ .

If we simply put  $\dot{\Delta} = \text{const}$ , ignoring its time modulation (see Eq. (A8)), the time averaged amplitude is estimated to be

$$\langle \mathcal{A}_{\text{total}}^2 \rangle^{1/2} = h(1 + F^2)^{1/2}. \quad (41)$$

We will use this expression later in §6.

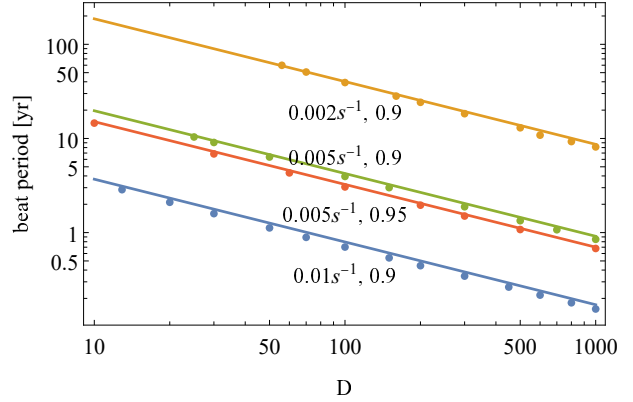


**Figure 5.** The beat periods  $T_b$  for the parameter combinations  $(n [s^{-1}], M_s [M_\odot]) = (0.002, 0.90)$ ,  $(0.005, 0.90)$ ,  $(0.01, 0.90)$  and  $(0.005, 0.95)$  all with the fixed value  $M_p = 1.0M_\odot$ . The points are obtained from numerical experiments and the solid lines are the analytical expressions given by Eq. (43).

#### 5 BEAT PERIOD

As discussed in the previous section, the drifting solution generates amplitude variation of gravitational waves due to a beat effect. The beat period  $T_b$  is given by the mean drift rate  $A$  as

$$T_b = \pi/A. \quad (42)$$

For example, we have  $T_b \sim 10$  yr for the system discussed in §3.3 with  $D = 25$ . This period would be suitable for observation by LISA (Amaro-Seoane et al. 2012). Considering these aspects, in this section, we specifically study the drift rate  $A$  or equivalently the beat period  $T_b$ . Since our model is a highly simplified one, we do not necessarily take the actual numerical values too seriously. Instead, together with Appendix A, our discussion would help us to analytically understand the underlying structure of the drifting solution.

So far, we have mainly examined the system with  $n \simeq 0.005 s^{-1}$  and  $(M_p, M_s) = (1.0M_\odot, 0.90M_\odot)$  for which drifting solutions are realized at  $D \gtrsim 24$  as shown in Fig. 2. For comparison, we additionally study the following three cases;  $(n [s^{-1}], M_s [M_\odot]) = (0.002, 0.90)$ ,  $(0.01, 0.90)$  and  $(0.005, 0.95)$  all with  $M_p = 1.0M_\odot$ . The minimum coupling parameters  $D$  for the drifting solutions are 13, 56 and 5.9 respectively.

In Fig. 5, we show the beat periods  $T_b$  that were numerically obtained for various sets of the coupling parameters  $D$  above the thresholds for the synchronization capture. In this log-log plot, we can clearly observe the power-law relations  $T_b \propto D^{-2/3}$ . Indeed, in Appendix A, we derive the following analytical expression for the drift rate

$$A' = 2^{-1/9} 3^{8/9} D^{2/3} (F - 1)^{-1/3} n^{4/9} t_{\text{gw},s}^{-5/9} \quad (43)$$

with the prime ' temporarily added to show the analytical counterpart to the original quantity  $A$ . For this derivation, we extracted the oscillating components of the mass transfer rates and the semi-major axes, induced by the Newtonian torque. Then we solve the drift rate  $A'$  by using the energy balance equation (30). In Fig. 5, we added the analytical estimation  $T_b = \pi/A'$  as four curves. It well reproduces the numerical results.

Next, we briefly discuss the long-term evolution of

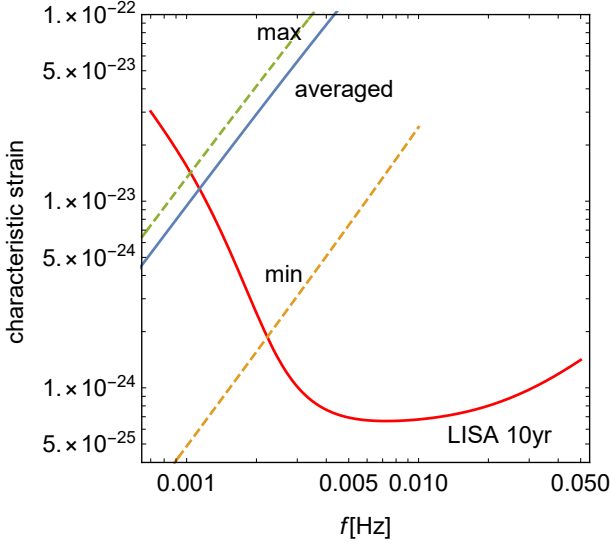


**Figure 6.** The three characteristic strain amplitudes of a drifting system with the total masses  $(M_p, M_s) = (1.0M_\odot, 0.90M_\odot)$  and the distance  $D_L = 5\text{kpc}$ . The upper dashed line is the maximum amplitude at  $\cos 2\Delta = 1$ , and the bottom dashed line is the minimum one at  $\cos 2\Delta = -1$ . The blue solid line is the time averaged amplitude. The effective noise levels  $\sqrt{S_n(f)T_{\text{obs}}^{-1}}$  of LISA is given for the observation period  $T_{\text{obs}} = 10\text{yr}$ , and contains the Galactic confusion noise.

a drifting system with a given inter-binary separation  $d$ . The evolution timescale is approximately given by  $t_{\text{gw,p}}$  in Eq. (6). Using the relation (11) for the donor mass, we have  $t_{\text{gw,p}} \propto n^{-11/3}$ . Then, from Eqs. (22) and (43), we have  $A' \propto d^{-10/3} n^{-23/27}$ . For the specific mass parameters  $(M_p, M_s) = (1.0M_\odot, 0.90M_\odot)$ , we obtain the beat period

$$T_b = 10(d/0.13\text{AU})^{10/3} (n/0.005\text{s}^{-1})^{23/27} \text{yr}. \quad (44)$$

## 6 OBSERVATION WITH LISA

In this section, we discuss observation of a drifting four-body system with LISA. Here, instead of the orbital angular velocity  $n$ , we use the gravitational wave frequency  $f = n/\pi$ .

For an isolated circular binary, after taking its direction and orientation averages, the effective strain amplitude  $h$  is given by

$$h = \frac{8(GM)^{5/3} \pi^{2/3} f^{2/3}}{5^{1/2} c^4 D_L} \quad (45)$$

with the chirp mass  $\mathcal{M}$  and the binary distance  $D_L$  (see e.g. Robson, Cornish & Liu 2019).

As shown in Eq. (40), a drifting system changes its gravitational wave amplitude  $\mathcal{A}_{\text{total}}$  between  $h(F-1)$  and  $h(F+1)$  with the time averaged value  $h(F^2+1)^{1/2}$  given in Eq. (41).

In Fig. 6, we plot the three amplitudes for the model parameters  $(M_p, M_s) = (1.0M_\odot, 0.90M_\odot)$  and  $D_L = 5\text{kpc}$ . In this plot, the factor  $F \equiv (M_p/M_s)^{5/3}$  depends very weakly on  $f$ . In fact, when the donor masses are much smaller than accretor masses, we have  $F \simeq (M_p/M_s)^{2/3} \sim \text{const.}$  For the

present model parameters, we get  $F \sim 1.05$ , and the amplitude changes by a factor of  $(F+1)/(F-1) \sim 40$  during the single beat period.

If the beat period  $T_b$  is smaller than the observation period  $T_{\text{obs}}$ , the optimal signal-to-noise ratio of the emitted waves can be evaluated with the averaged amplitude as

$$SNR \simeq \frac{h(F^2+1)^{1/2}}{\sqrt{S_n(f)T_{\text{obs}}^{-1}}}. \quad (46)$$

Here  $S_n(f)$  is the standard strain noise spectrum of LISA and defined in units of  $[\text{Hz}^{-1}]$  (Robson, Cornish & Liu 2019). In Fig. 6, for  $T_{\text{obs}} = 10\text{yr}$ , we show the effective noise levels  $\sqrt{S_n(f)T_{\text{obs}}^{-1}}$ . Applying Eq. (46) to our model parameters above, we have  $SNR = 67$  at  $f = 3.2\text{mHz}$  and 12 at  $2\text{mHz}$ .

For detecting the amplitude modulated waves with LISA, we consider the following two step data analysis. The first step is selecting candidates of drifting systems, using relatively short-term data. The next step is the follow-on examination of the candidates whether they have long-term amplitude modulations. For the first step, we can perform a matched filtering analysis, approximately using the short-term templates made for standard nearly monochromatic isolated binaries. For example, in the  $3.2\text{mHz}$  case above, we can get  $SNR \sim 8$  typically in the period  $10\text{yr} \times (8/67)^2 = 0.14\text{yr}$  that could be much smaller than the beat period. Another method for the first-step candidate selection is a search for localized power in a narrow frequency interval (see Cornish & Larson 2003 for the Doppler demodulation). In reality, the candidates after the first step will be dominated by simple isolated binaries. But, after the second step, we might identify a small number of drifting systems.

## 7 SUMMARY AND DISCUSSION

In this paper, using a very simple model based on Paczyński (1967) and Paczyński & Sienkiewicz (1972), we examine evolution of coupled dual mass-transferring WD binaries around the synchronization point  $n_p \sim n_s$ . We find that, in a strongly coupled configuration (i.e. short mutual distance), the system can asymptotically settle into a drifting solution as a limit cycle. This state is remarkably different from a synchronization capture realized in less strong coupling (Seto 2018).

Considering ‘‘stability’’ of the drifting solution against small perturbation as shown in Fig. 4, we can qualitatively expect that such solutions would be maintained to some extent, even adding small corrections to our simple model. But, to better understand what actually happens around the synchronization point, we need to quantitatively examine various physical effects that are not included in the present model. For example, our formulation is based on the balances of angular momenta. But, for each binary, as shown in Eq. (3), we only considered the orbital angular momentum essentially for two point masses. In reality, the angular momentum is partially stored in the spin rotations of the accretor and possibly in its accretion disk, or might be lost from the four-body system due to a mass loss (see e.g. Marsh et al. 2004; Gokhale et al. 2007; Solheim 2018). These corrections also affect the response of orbital angular velocity to externally added torque, and could play interesting roles



for the dynamical couplings. Meanwhile, we just included the resonant torques for the inter-binary interaction. But other short-term torques might disturb the ordered structures studied in this paper (see e.g. Murray & Dermott 1999 for the effects of non-resonant terms). In any case, our study here is far from complete, and additional effects are worth considering.

The drifting solution generates amplitude variation of emitted gravitational waves, due to a beat effect. Depending on model parameters, the beat period could be 1-10 yr and a large amplitude variation might be actually observed by LISA. In this respect, we might detect other associated signatures encoded in gravitational waveform such as a small phase modulation caused by the outer orbital motion.

In this paper, we concentrate our study around the synchronization point  $n_p \sim n_s$  where our formulation is applicable. It would be also interesting to discuss other evolutionary stages, especially possible pathways to forming strongly coupled four-body systems as considered in this paper. We left these issues as future works.

## ACKNOWLEDGEMENTS

the author would like to thank the reviewer for valuable comments on the manuscript. This work is supported by JSPS Kakenhi Grant-in-Aid for Scientific Research (Nos. 15K65075, 17H06358 and 19K03870).

## DATA AVAILABILITY

The data underlying this article will be shared on reasonable request to the corresponding author.

## REFERENCES

- Abbott B. P. et al., 2016, Phys. Rev. Lett., 116, 061102  
Amaro-Seoane P. et al., 2012, Classical and Quantum Gravity, 29, 124016  
Breiter S., Vokrouhlický D., 2018, MNRAS, 475, 5215  
Burke W. L., 1971, Journal of Mathematical Physics, 12, 401  
Cornish N. J., Larson S. L., 2003, CQGra, 20, S163  
Fang X., Thompson T. A., Hirata C. M., 2018, MNRAS, 476, 4234  
Fragione G., Kocsis B., 2019, MNRAS, 486, 4781  
Glanz H., Perets H. B., 2020, arXiv, arXiv:2004.00020  
Gokhale V., Peng X. M., Frank J., 2007, ApJ, 655, 1010  
Goldreich P., Peale S. J., 1968, AR&A, 6, 287  
Hamers A. S., Lai D., 2017, MNRAS, 470, 1657  
Iben I., Livio M., 1993, PASP, 105, 1373  
Maggiore M. Gravitational waves volume 1: theory and experiments, Oxford university press, 2008  
Mardling R. A., Aarseth S. J., 2001, MNRAS, 321, 398  
Marsh T. R., Nelemans G., Steeghs D., 2004, MNRAS, 350, 113  
Murray C. D., Dermott S. F., 1999, Solar system dynamics. Cambridge University Press  
Néda Z., Ravasz E., Brechet Y., Vicsek T., Barabási A.-L., 2000, Natur, 403, 849

- Nelemans G., Yungelson L. R., Portegies Zwart S. F., 2001, A&A, 375, 890  
Nelemans G., Yungelson L. R., Portegies Zwart S. F., 2004, Mon. Not. Roy. Astro. Soc., 349, 181  
Paczynski B., 1967, Acta, Astron., 17, 287  
Paczynski B., Sienkiewicz R., 1972, Acta. Astron., 22, 73  
Pikovsky A., Rosenblum M., Kurths J., 2003, Synchronization. Cambridge University Press  
Raghavan D., et al., 2010, ApJS, 190, 1  
Robson T., Cornish N. J., Liu C., 2019, CQGra, 36, 105011  
Sana H., et al., 2013, A&A, 550, A107  
Solheim J.-E., 2010, PASP, 122, 1133  
Seto N., 2018, MNRAS, 475, 1392  
Taam R. E., Sandquist E. L., 2000, ARA&A, 38, 113  
Thorne K. S., 1969, ApJ, 158, 997  
Tokovinin A., 2014, AJ, 147, 87  
Toonen S., Hamers A., Portegies Zwart S., 2016, ComAC, 3, 6  
Tremaine S., 2020, MNRAS, 493, 5583  
de Vries N., Portegies Zwart S., Figueira J., 2014, MNRAS, 438, 1909  
Webbink R. F., 1984, ApJ, 277, 355  
Zapolsky H. S., Salpeter E. E., 1969, ApJ, 158, 809

## APPENDIX A: ANALYTICAL EVALUATION FOR THE DRIFT RATE

In this appendix, we derive an analytical expression for the drift rate  $A \equiv |\dot{\Delta}|$ . This derivation would be useful also to understand the underlying structure of the drifting solution. We assume  $D \gg 1$  and put  $F = 1$ , except for the combination  $(F - 1)$ .

During the drift, the two binaries exchange angular momenta with the Newtonian torque  $T_p = -T_s \propto \sin 2\Delta$  (see Eq. (13)) at the mean angular speed  $2A$ . Our basic strategy here is (i) to derive relations for the oscillating components of  $(\dot{m}_{p2}, \dot{m}_{s2})$  and  $(a_p, a_s)$  induced by the exchange, and (ii) to subsequently estimate the drift rate  $A$  by using the averaged energy variation rate.

To begin with, for the mass transfer rate  $\dot{m}_{p2}$ , we decompose the nearly constant (DC) part  $\bar{\dot{m}}_{p2}$  and the oscillating (AC) part  $\delta\dot{m}_{p2}$  as follows

$$\dot{m}_{p2} = \bar{\dot{m}}_{p2} + \delta\dot{m}_{p2}. \quad (\text{A1})$$

Similarly, we separate the inner semi-major axis into the smooth part  $\bar{a}_p$  and the oscillating part  $\delta a_p$

$$a_p = \bar{a}_p + \delta a_p. \quad (\text{A2})$$

Next, by perturbatively expanding Eq. (9) and using Eq. (12), we obtain the following expression

$$\frac{\delta\dot{m}_{p2}}{m_{p2}} = 6n \frac{\delta a_p}{a_p} \left( \frac{-\bar{\dot{m}}_{p2}}{2nm_{p2}} \right)^{2/3} = 6n \frac{\delta a_p}{a_p} \left( \frac{3}{4t_{\text{gw},s}n} \right)^{2/3}. \quad (\text{A3})$$

Here we neglected the contribution of  $\delta m_{p2}$  on the right-hand side of Eq. (12) (as justified shortly) and also dropped the step function (as already commented after Eq. (9)). For the magnitudes of oscillation amplitude, we have

$$\frac{\delta\dot{m}_{p2}}{m_{p2}} \sim \frac{\delta\dot{a}_p}{a_p} \left[ \frac{3n}{A} \left( \frac{3}{4t_{\text{gw},s}n} \right)^{2/3} \right] \ll \frac{\delta\dot{a}_p}{a_p}. \quad (\text{A4})$$

In the above relation, we use the fact that the factor  $[\dots]$  is much smaller than unity for the actual numerical data  $A$  shown in Fig. 5. After taking time integration, we can expect a similar hierarchy for  $\delta m_{p2}/m_{p2} \ll \delta a_p/a_p$ , justifying the expansion of Eq. (A3) only with  $\delta a_p/a_p$ . From Eqs. (23) and (A4), we have

$$\frac{\delta \dot{a}_p}{a_p} = \frac{2D}{t_{\text{gw},s}} \sin(2\Delta). \quad (\text{A5})$$

For the secondary binary, we can show similar relations

$$\frac{\delta \dot{m}_{s2}}{m_{s2}} = 6n \frac{\delta a_s}{a_s} \left( \frac{3}{4t_{\text{gw},s}n} \right)^{2/3}, \quad (\text{A6})$$

$$\frac{\delta \dot{a}_s}{a_s} = -\frac{2D}{t_{\text{gw},s}} \sin(2\Delta). \quad (\text{A7})$$

Integrating Eq. (26) after using Eqs. (A5) and (A7), we have

$$\dot{\Delta} = -A - \frac{3nD}{t_{\text{gw},s}A} \cos(2\Delta). \quad (\text{A8})$$

Here we applied the condition  $A \equiv |\bar{\Delta}|$  for determining the integral constant, and put  $\int^t \sin 2\Delta dt = -(2A)^{-1} \cos 2\Delta$  for the correction term. From Eqs. (A3) and (A6), keeping the term relevant for the arguments below, we have

$$\frac{\delta \dot{m}_{p2}}{m_{p2}} - \frac{\delta \dot{m}_{s2}}{m_{s2}} = C \cos(2\Delta) \quad (\text{A9})$$

with

$$C = 12 \frac{nD}{t_{\text{gw},s}A} \left( \frac{3}{4t_{\text{gw},s}n} \right)^{2/3}. \quad (\text{A10})$$

Now, we solve the unknown parameter  $A$ , by evaluating the long-term energy variation rate  $\dot{E}$  in two different ways. First, using the steady drift of potential energy (through its linear term), we have

$$\bar{\dot{E}} = \frac{\partial \bar{V}}{\partial \Delta} \bar{\Delta} = -\frac{3An(F-1)}{t_{\text{gw},s}} \quad (\text{A11})$$

Meanwhile, using Eq. (30) and taking the time average of the following combination

$$3n \left( \frac{\delta \dot{m}_{p2}}{m_{p2}} - \frac{\delta \dot{m}_{s2}}{m_{s2}} \right) \dot{\Delta}, \quad (\text{A12})$$

we have

$$\bar{\dot{E}} = -\frac{9Dn^2C}{2At_{\text{gw},s}}. \quad (\text{A13})$$

Here, in the asymptotic stage, the constant parts ( $\bar{m}_{p2}$ ,  $\bar{m}_{s2}$ ) are expected to be almost canceled in Eq. (30) and we only kept the oscillating (anti-phase) parts, ignoring the small parameter  $q_p \sim q_s \ll 1$ . Matching Eqs. (A11) and (A13), we finally obtain

$$A = 2^{-1/9} 3^{8/9} D^{2/3} (F-1)^{-1/3} n^{4/9} t_{\text{gw},s}^{-5/9}. \quad (\text{A14})$$